

A semi-diagnostic calculation of climatic circulation in the western Indian Ocean

C Shaji, N Bahulayan*, S K Dube & A.D.Rao

Centre for Atmospheric Sciences, Indian Institute of Technology, Hauz Khas, New Delhi 110016, India

*Physical Oceanography Division, National Institute of Oceanography, Dona Paula, Goa 403004, India

Received 17 September 1996; revised 10 February 1997

A 3-dimensional, semi-diagnostic circulation model is used to compute the climatic circulation in the upper levels of western tropical Indian Ocean (20°S-30°N and 35°E-80°E) during the premonsoon month of May. The model involves the sea surface topography function used as the integral function, and is driven with the wind stress at the surface and thermohaline forcing at different levels. A steady state solution is obtained within 40 days of model integration. Computed currents are compared with available observations on currents at selected regions in the model area and it has been found that both agreed fairly well. Computed results are also explained in terms of the model forcing parameters and the dynamics considered in the model.

The circulation in the tropical Indian Ocean is unique among other major oceans in the same latitude. Seasonal reversal of surface wind field over the tropical Indian Ocean is the most dramatic one than in other regions of the low latitude. This wind reversal has profound effects on the upper hydrographic structure and the seasonal variation of surface current systems in the Indian Ocean. Many of the observational and modelling investigations have concentrated on the northwestern Indian Ocean, with relatively little attention paid to the other regions. Local forcings of wind and vertical density variation play a significant role in driving the 3-D circulation in the Indian Ocean.

Semi-diagnostic ocean circulation models are effective tools to compute the climatological mean circulation and to understand the role of local forcings in driving the circulation. Pioneering works in the field of semi-diagnostic modelling were carried out by Marchuk & Sarkisyan¹. There have been a number of other outstanding works on the semi-diagnostic calculation of large scale circulation in the world oceans^{2,3}. In the present study, a 3-D semi-diagnostic circulation model is used to compute the climatic circulation in the western part of tropical Indian Ocean during May, a representative month for premonsoon season.

Materials and Methods

The present model (20°S-30°N and 35°E-80°E) has a maximum depth of 900 m, a resolution of 1° in the zonal and meridional directions and 18 levels in the vertical which are standard oceanographic depths. Model equations are based on the basic hydrothermodynamic equations in spherical co-ordinate system governing the large scale 3-dimensional circulation in the ocean given by Gill⁴. These equations are then modified in terms of co-latitude of the place and particular sign convention used in the model wherein the longitude (λ) increases towards east, the co-latitude (θ) increases towards south and vertical co-ordinate (z) increases downwards. The final model equations assuming approximations of Boussinesq, hydrostatics and incompressibility of seawater are:

$$\frac{\partial u}{\partial t} + Au + lv + \cot \theta \frac{uv}{R} = -\frac{1}{\rho_o R \sin \theta} \frac{\partial p}{\partial \lambda} + F^\lambda \quad \dots (1)$$

$$\frac{\partial v}{\partial t} + Av - lu - \cot \theta \frac{u^2}{R} = -\frac{1}{\rho_o R} \frac{\partial p}{\partial \theta} + F^\theta \quad \dots (2)$$

$$\frac{\partial p}{\partial z} = g\rho \quad \dots (3)$$

$$\frac{1}{R \sin \theta} \left[\frac{\partial u}{\partial \lambda} + \frac{\partial (v \sin \theta)}{\partial \theta} \right] + \frac{\partial w}{\partial z} = 0 \quad \dots (4)$$

$$\rho = \rho(T, S) \quad \dots (5)$$

$$\frac{\partial T}{\partial t} + AT = \frac{\partial [v_T \frac{\partial T}{\partial z}]}{\partial z} + \mu_T \Delta T \quad \dots (6)$$

$$\frac{\partial S}{\partial t} + AS = \frac{\partial [v_S \frac{\partial S}{\partial z}]}{\partial z} + \mu_S \Delta S \quad \dots (7)$$

where

θ —co-latitude = $90 - \phi$, ϕ is the latitude

u, v, w —the velocity components along the east(λ), south(θ) and downward (z) directions respectively

p —hydrostatic pressure

ρ —density of sea water

ρ_0 —constant density

R —radius of the Earth

l — $2\Omega \cos \theta$

Ω —angular velocity of Earth's rotation

Au, Av —advective acceleration terms in the momentum equations

F^λ, F^θ —friction terms in the momentum equations

μ, ν —horizontal and vertical eddy viscosity coefficients respectively

μ_h, ν_h —horizontal and vertical eddy diffusivity coefficients of heat and salt

T —temperature

S —salinity

$$Af = \frac{1}{R \sin \theta} \left[\frac{\partial (uf)}{\partial \lambda} + v \frac{\partial (f \sin \theta)}{\partial \theta} \right] + \frac{\partial (wf)}{\partial z}$$

$$F^\lambda = \frac{\partial \left(v \frac{\partial u}{\partial z} \right)}{\partial z} + \mu \left[\Delta u - \frac{u}{R^2 \sin^2 \theta} + \frac{2 \cos \theta}{R^2 \sin^2 \theta} \frac{\partial v}{\partial \lambda} \right]$$

$$F^\theta = \frac{\partial \left(v \frac{\partial v}{\partial z} \right)}{\partial z} + \mu \left[\Delta v - \frac{v}{R^2 \sin^2 \theta} + \frac{2 \cos \theta}{R^2 \sin^2 \theta} \frac{\partial u}{\partial \lambda} \right]$$

$$\Delta f = \frac{1}{R^2 \sin^2 \theta} \frac{\partial^2 f}{\partial \lambda^2} + \frac{1}{R^2 \sin \theta} \frac{\partial (\sin \theta \frac{\partial f}{\partial \theta})}{\partial \theta}$$

The following boundary conditions are used for the velocity fields (u, v, w), temperature (T) and salinity (S) at the ocean surface ($z=0$).

$$\begin{aligned} \rho_0 v \frac{\partial u}{\partial z} &= -\tau_\lambda; \rho_0 v \frac{\partial v}{\partial z} = -\tau_\theta; w|_{z=0} \\ &= 0; T|_{z=0} = T^*; S|_{z=0} = S^* \end{aligned} \quad \dots (8)$$

where τ_λ and τ_θ are the components of wind stress in the zonal and meridional directions respectively; u, v are the velocity components and T^* and S^* are the observed temperature and salinity data at the surface.

At the bottom $z=H(\lambda, \theta)$, a non-slip boundary condition is used for the velocity fields.

$$i.e. \quad u = v = w = 0 \quad \dots (9)$$

For temperature and salinity, their fluxes are zero at the bottom.

$$\frac{\partial T}{\partial z} = \frac{\partial S}{\partial z} = 0 \quad \dots (10)$$

Along the rigid lateral boundaries, the boundary condition takes the following form

$$i.e. \quad \vec{v}_n = 0 \quad \dots (11)$$

$$\frac{\partial T}{\partial \vec{n}} = \frac{\partial S}{\partial \vec{n}} = 0 \quad \dots (12)$$

where ' \vec{n} ' is the normal to the boundary.

At the open sea boundaries, the velocity components computed with the help of a quasi-geostrophic model of Marchuk & Sarkisyan¹ were used.

The temperature and salinity at the open sea boundaries were given as:

$$T|_L = T^*; S|_L = S^* \quad \dots (13)$$

where T^* and S^* are the climatic temperature and salinity data.

An initial state of rest is prescribed at time $t=0$.

$$(u, v)_{t=0} = 0; (T, S)_{t=0} = (T^*, S^*) \quad \dots (14)$$

The density of seawater ' ρ ' is the sum of the average density ' ρ_0 ' and the density anomaly $\rho'(\lambda, \theta, z)$. Integrating the hydrostatic Eq. (3) over the vertical from free surface to depth z , the hydrostatic pressure at depth z becomes :

$$p_z = \rho_0 g \zeta + g \int_0^z \rho' dz \quad \dots (15)$$

where ' ζ ' is the sea surface topography or sea level. An additional equation for sea surface topography (sea level) has to be derived to have a closed system of 8 model equations in 8 unknown variables.

Equations (1)-(7) are solved by means of a leap-frog numerical scheme. By adding the equation of continuity over the vertical levels after considering the boundary condition at the surface and bottom for vertical velocity (ie. $w=0$), the two-dimensional integral continuity equation which is the equation for sea surface topography at the internal grid points is obtained. The sea surface topography equation at the solid boundary points are obtained by giving the lateral boundary condition for velocity field in the two-dimensional integral continuity equation. The two-dimensional integral continuity equation at the internal grid point is:

$$\frac{1}{R \sin \theta} [\delta_\lambda \bar{u}^\theta + \delta_\theta \bar{v} \sin \theta^\lambda] = 0 \quad \dots (16)$$

where δ_λ and δ_θ are the finite difference operators and \bar{u} and \bar{v} are the vertically integrated velocity

components in the zonal and meridional direction respectively. Substituting the values of \bar{u} and \bar{v} in the integral continuity equation, we get the equation for sea surface topography as follows:

$$\frac{1}{R \sin \theta} \left[\frac{\delta_\lambda (a \delta_\lambda \bar{\zeta}^\theta + b \delta_\theta \bar{\zeta}^\lambda)}{\delta_\theta (a \delta_\theta \bar{\zeta}^\lambda - b \delta_\lambda \bar{\zeta}^\theta)} \right] \sin \theta = R_s \quad \dots (17)$$

where

$$a = \frac{\Delta t g H}{1 + \left(\frac{\Delta t^2 l^2}{4} \right)}$$

$$b = a l \frac{\Delta l}{2}$$

$$R_s = \frac{1}{R \sin \theta} \left[\delta_\lambda \bar{R}_\lambda^\theta + \delta_\theta (\bar{R}_\theta^\lambda \sin \theta) \right]$$

$$R_\lambda = R_u - \frac{\left(\frac{\Delta l}{2} R_v \right)}{\left(1 + \frac{\Delta t^2 l^2}{4} \right)}$$

$$R_\theta = R_v + \frac{\left(\frac{\Delta l}{2} R_u \right)}{\left(1 + \frac{\Delta t^2 l^2}{4} \right)}$$

$$R_u = u^{n-1} + \Delta t \left[-\frac{l v^{n-1}}{2} - \left(\frac{g}{\rho_0 R \sin \theta} \int_0^z \frac{\partial \rho'}{\partial \lambda} dz - Au - \cot \theta \frac{uv}{R} \right)^n + (F^\lambda)^{n-1} \right]$$

$$R_v = v^{n-1} + \Delta t \left[\frac{l u^{n-1}}{2} - \left(\frac{g}{\rho_0 R} \int_0^z \frac{\partial \rho'}{\partial \theta} dz - Av - \cot \theta \frac{u^2}{R} \right)^n + (F^\theta)^{n-1} \right]$$

where Δt is the time step and n is the time step number.

The sea surface topography Eq. (17) is solved by successive overrelaxation technique. The relaxation parameter used for solving the above equation is 1.0.

Results and Discussion

Solution procedure and model forcing parameters

In the semi-diagnostic method, the steady state solution of the complete set of model equations [Eqs (1)-(7)] is obtained in two stages on a 46×51 staggered grid. In the first stage, called the diagnostic stage, all the equations except turbulent diffusion equations of heat and salt are solved subject to proper boundary and initial conditions mentioned above using a leap-frog numerical scheme. To inhibit time-splitting instability normally encountered in the leap-frog scheme, a Matsuno scheme which averages solution at two consecutive time steps was employed at every 24 time steps. Equations are integrated forward in time with a time step Δt of 1 hour for approximately 20 days to obtain a quasi-steady solution for velocity field. The density is kept constant throughout the diagnostic stage. In the second stage, which is called adaptation or initialization, the diagnostic equations together with the turbulent diffusion equations of heat and salt are again solved using the velocity field obtained during the first stage and original temperature and salinity fields as initial conditions. The integration of the complete set of model equations is again continued for another 20 days to obtain a steady state solution. The total period of integration for both diagnostic and initialization calculation is 40 days. The parameter values used for the horizontal eddy viscosity (μ) and eddy diffusivity (μ_v) coefficients in the model are $5 \times 10^8 \text{ cm}^2 \text{ sec}^{-1}$, whereas the values for vertical eddy viscosity (ν) and eddy diffusivity (ν_v) coefficients are $10 \text{ cm}^2 \text{ sec}^{-1}$.

To calculate the monthly mean circulation and sea surface topography using the above semi-diagnostic model, monthly mean wind stress and monthly mean density field at various levels are required. The monthly mean wind data used in the present study come from Hellerman & Rosenstein⁵ who prepared the global wind stress field on a

$2^\circ \times 2^\circ$ square. These data were further interpolated to 1° resolution by means of a bilinear interpolation technique for the model area (20°S - 30°N and 35°E - 80°E). Results of sea surface topography and circulation at 10, 50, 150, 500 and 700 m depths in the upper levels of the ocean for the month of May is discussed in this paper. The spatial distribution of mean resultant wind stress during May is presented in Fig. 1. The winds in the northern Arabian Sea and between equator and 5°N are westerlies with the exception of northwesterlies between equator to 5°N , west of 60°E longitude. Northwesterly winds with magnitudes less than 1 dynes cm^{-2} are seen in the southeastern Arabian Sea between 63°E and 75°E longitudes. In the southern hemisphere, between 0 and 5°S , a weak north, northeast or northwest wind stress is observed. The southern hemisphere between 5°S and 20°S is covered by either southeasterly or easterly trades whose maximum magnitude exceeds greater than 1 dynes cm^{-2} .

Levitus⁶ monthly mean data on temperature and seasonal mean salinity was used to provide thermohaline forcing in the model. Figure 2

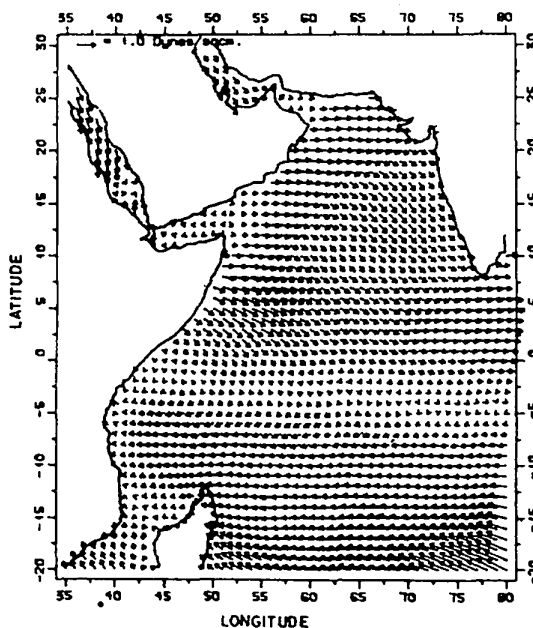
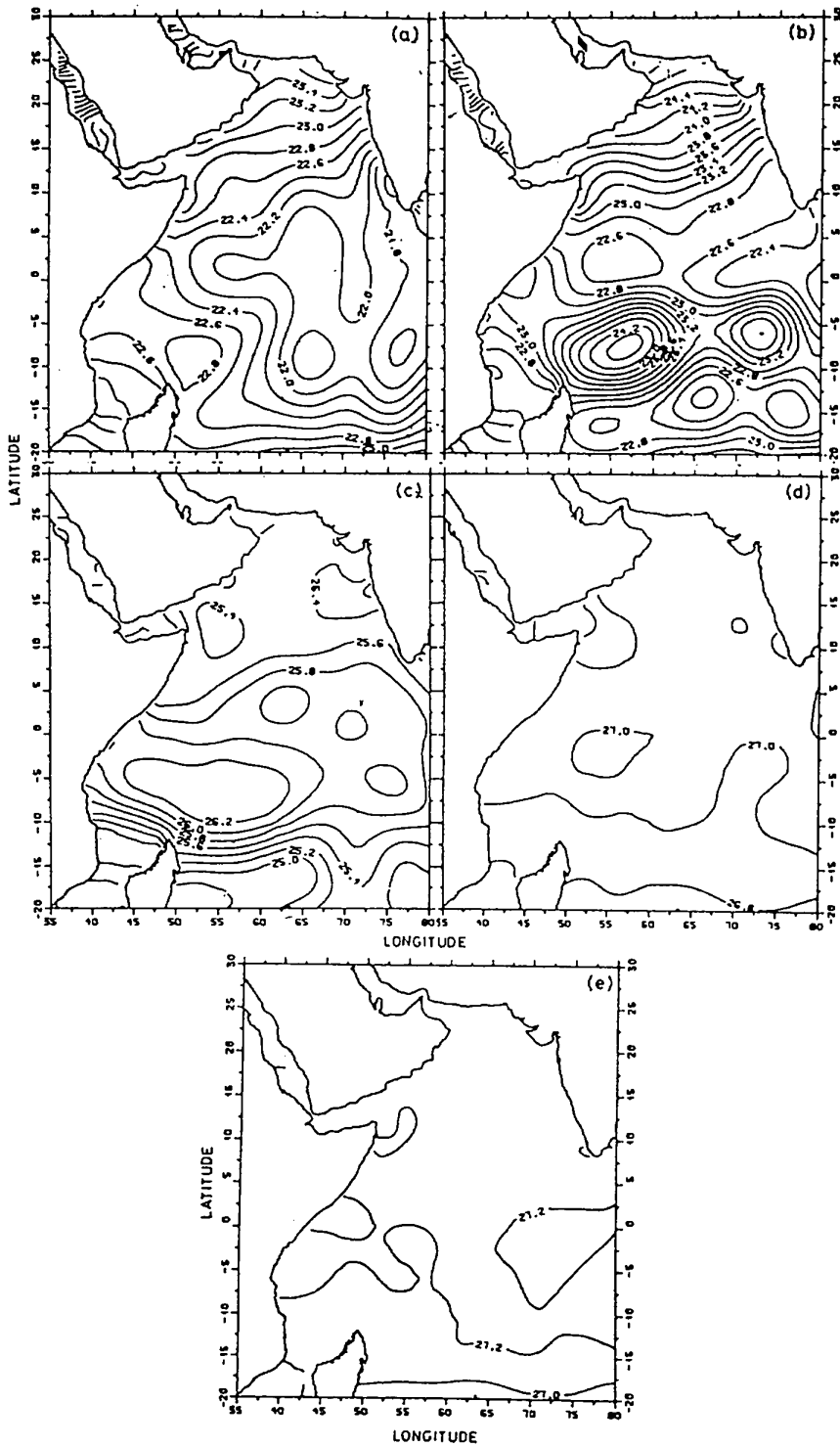


Fig. 1—Spatial distribution of May mean resultant wind stress (dynes cm^{-2})



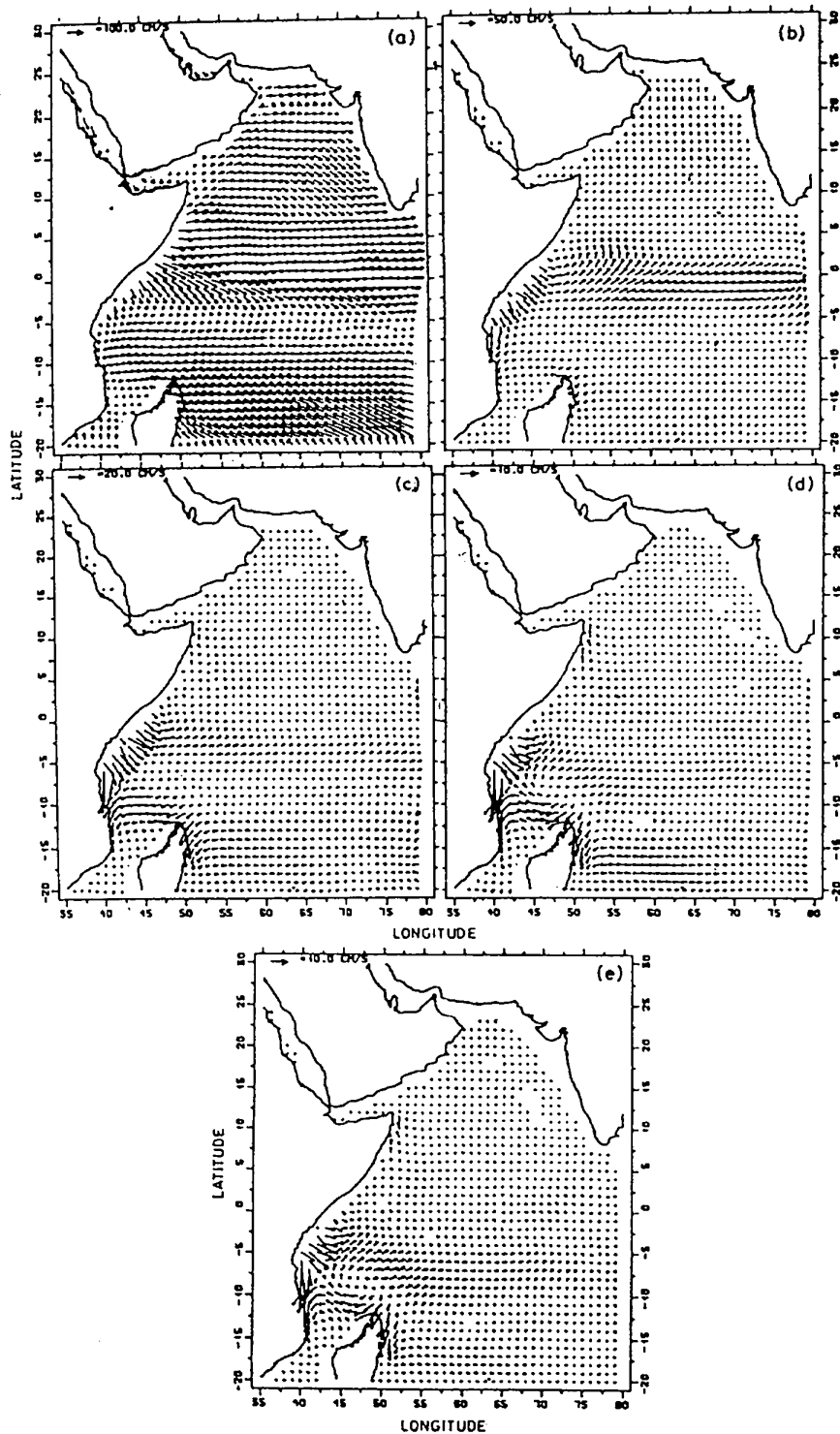


Fig. 3—Computed circulation during May at (a) 10 m depth (b) 50 m depth (c) 150 m depth (d) 500 m depth and (e) 700 m depth

represents the spatial distribution of σ_t fields at 10, 50, 150, 500 and 700 m depths. Figure 2a shows high dense water at the northern tip of Somalia due to the presence of cold upwelled water at the beginning of SW monsoon in May. High dense water can be seen in Figure 2a off the coasts of Arabia due to the presence of high saline water in this region. Figure 2b at 50 m depth also shows high dense water at the northern tip of Somali and along the Arabian coasts. The temperature gradually increases towards east and hence low dense water is observed off the southwest coast of India and central equatorial Indian Ocean at 10 and 50 m depths. In the southern hemisphere, high dense water with σ_t value of 24.6 is observed at 50 m depth at the southwestern sector of the model domain. The hydrographic study of Sastry & D'Souza⁷ shows high salinity values in this region. The high density values can be attributed to the observed high salinity values. The same high dense water can be seen at 150 m depth also. The density distribution is found to be more or less uniform at the deeper depths 500 and 700 m. The isopycnals are zonal in the southern hemisphere at 150, 500 and 700 m depths.

Computed circulation and sea surface topography

The model computed currents at 10, 50, 150, 500 and 700 m depths are depicted in Fig. 3 whereas Fig. 4 shows the computed sea surface topography. The computed currents are compared with the climatological currents of Cutler & Swallow⁸ and other observations. The ship drift measurements of surface currents have been compiled by Cutler & Swallow⁸. The original ship drift currents available at 10 day interval is averaged for each month and then interpolated to the model resolution of $1^\circ \times 1^\circ$ grid by means of a cubic spline technique. This diagram (Fig.5) is used for a possible comparison of the model computed current at 10 m.

The computed surface current regime at 10 m in the model area (Fig.3a) almost follow the climatological wind field used to drive the model. The broad westward flowing South Equatorial Current (SEC) ranges between 5°S and 20°S with velocities greater than 100 cm sec^{-1} at the southern part. The thickly packed zonally oriented sea surface topography contours between 10°S and 20°S in Fig.4 also reflect the presence of SEC in the model area. The SEC is found in all the other,

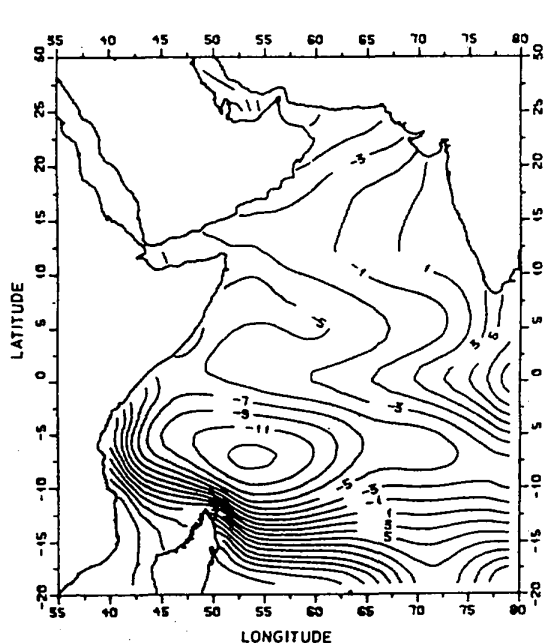


Fig. 4—Computed sea surface topography (cm) during May

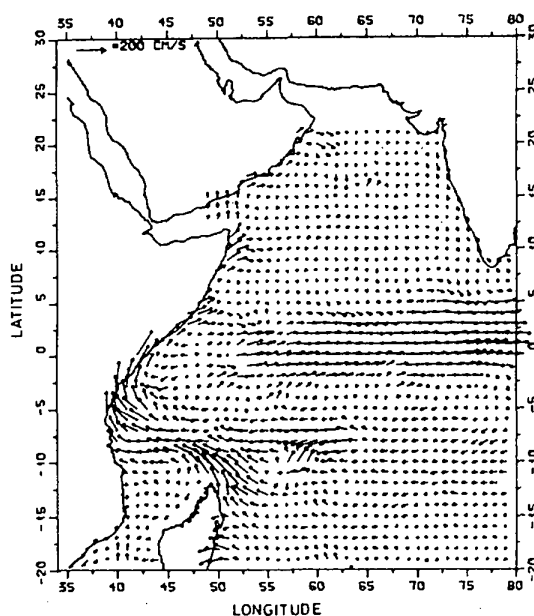


Fig. 5—The ship drift surface current of Cutler and Swallow for May

depths also (Fig. 3b-e) with the intensity of current reduced downwards. Another peculiarity of computed current during May is the presence of eastward Equatorial Jet (EJ) between 5°N and 3°S at 10 m depth. Occurrence of EJ in the tropical Indian Ocean during the transition period has been reported first by Wyrki⁹, and Molinari *et al.*¹⁰ also observed the same in the monthly climatology of surface currents using surface drifting buoy data. The EJ is forced by westerly winds and its velocity is of the order of 100 cm sec⁻¹. The northern tip of Somalia shows the northeastward flowing Somali Current. The northern Arabian Sea is mainly covered by eastward flow with a maximum velocity of 50 cm sec⁻¹. There is southeastward flow at the southeastern sector of the Arabian Sea along the west coast of India. The sea surface topography contours in Fig.4 show high sea level in this region due to the presence of low dense water and hence a weak northward flow is expected. However the computed southeastward flow can be interpreted as due to the northwesterly winds which dominate the effect of sea level and baroclinic forcing. The climatic features computed by the model such as the broad SEC, narrow EJ, eastward flow in the northern Arabian Sea and southeastward flow at the eastern sector of the Arabian Sea is in consistent with the ship drift currents in Fig. 5 and also with the model results of McCreary *et al.*¹¹, except the formation of eddies at the eastern Africa and Somali coasts. These eddy-like features can be resolved only in prognostic simulation models of climatic circulation with the incorporation of more real time surface forcing functions. Simulation of eddies are also sensitive to the model resolution and the model parameters such as the more realistic parameterisation of the eddy coefficients.

The SEC and EJ computed at 10 m depth is found at 50 m depth also (Fig. 3b), otherwise the current pattern at 50 m is different from the one at 10 m. The SEC now ranges between 10°S and 20°S with less intensity. The presence of huge Madagascar island splits the SEC at 50 to 700 m depths, and there is southward flow east of Madagascar as the East Madagascar Current (EMC) (Fig. 3b-e), and west of Madagascar there is southward flow along the African coast (Fig. 3c,d). South of 6°S, the model computed a

southward flow along the African coast which may be due to baroclinic pressure gradient force. These southward flows along the east Madagascar and south of 6°S along the African coast is found in the other depths at 150, 500 and 700 m (Fig. 3c-e) also and are in consistent with the numerical simulation of McCreary *et al.*¹¹. The EJ at 50 m depth (Fig. 3b) ranges between 3°N and 3°S, and is driven by the westerlies and high sea level off the African coast. There is a weak westward flow between the southwest coast of India and northern Somali. At the northern tip of Somali, the current shows a tendency to flow southward. This can be interpreted as the Somali Undercurrent. Observational evidence of Quadfasel & Schott¹² showed a weak Somali Undercurrent at the surface layer and its absence at the subsurface levels. However, the model study of Jensen¹³ showed the absence of Somali Undercurrent during spring season. The flow north of 15°N at 50 m depth is mainly northeastward. At the northern most Arabian Sea, there is a weak eastward flow which shows the entrance of high saline Red Sea water at subsurface level into this region.

The Fig. 3c at 150 m depth shows an Equatorial Undercurrent (EUC) between equator and 5°S. The southward Somali Undercurrent is not exhibited in this depth, instead there is northward flow at the northern tip of Somali which is well observed at 500 and 700 m also. Along the west coast of India, the model computed a weak northward undercurrent. The same has been observed by Shetye *et al.*¹⁴ in their dynamic computations of currents using hydrographic data.

At 500 m depth, the SEC and EUC has shifted more to the south (Fig.3d). The SEC now extends between 15°S and 20°S and is seen more significantly in the western part between 52°E and 65°E. The EUC is seen between 5°S and 10°S. There is no substantial difference in the current pattern between 500 and 700 m depth, except that the intensity of current is further reduced at 700 m.

Acknowledgement

The authors express their gratitude to the Head, Centre for Atmospheric Sciences, IIT, New Delhi and Head, Data Division, NIO, Goa for facilities. C. Shaji also acknowledges the CSIR, New Delhi

for awarding a Senior Research Fellowship to carry out this work.

References

- 1 Marchuk G I & Sarkisyan A S, *Mathematical modelling of ocean circulation* (Springer-Verlag, Berlin), 1988,292.
- 2 Sarkisyan A S & Demin Yu L, *A semi-diagnostic method of sea current calculations* (Large scale oceanographic experiments in the WCRP Publication, Tokyo), 1983,201.
- 3 Demin Yu L & Ibraev R A, *Sov J Numer Anal Math Modelling*,4,3 (1989), 211.
- 4 Gill A E , *Atmosphere-ocean dynamics* (Academic Press, New York), 1982, pp. 662.
- 5 Helleman S & Rosenstein M, *J Phys Oceanogr* ,13 (1983), 1093.
- 6 Levitus S , *Climatological atlas of the world ocean*, NOAA, Prof. paper 13, (US Govt. Printing Office, Washington D.C.), 1982,173.
- 7 Sastry J S & D'Souza R S, *Indian J Met Geophys*, 21 (1972), 367.
- 8 Cutler A N & Swallow J C, *Surface currents of the Indian Ocean* (Institute of Oceanographic Sciences, U K), 1984, pp.8.
- 9 Wyrtki K, *Oceanographic Atlas of the International Indian Ocean Expedition*, (NSF, Washington D C), 1971, pp. 531.
- 10 Molinari R L, Olson D & Reverdin G, *J Geophys Res*,94,C5 (1990), 7217.
- 11 McCreary J P, Kundu P K & Molinari R L, *Progr Oceanogr*,31 (1993), 181.
- 12 Quadfasel D R & Schott F, *J Geophys Res* ,88,C10 (1983), 5973.
- 13 Jensen T G, *J Geophys Res*,96, (1991), 22151.
- 14 Shetye S R, Gouveia A D, Shenoi SSC, Sundar D, Michael G S, Almeida A M & Santanani K, *J Mar Res*,48, (1990), 359.